



TITLE:

# Direct Observation of Rate Determining Step for Nd<sub>2</sub>NiO<sub>4+δ</sub> SOFC Cathode Reaction by operando Electrochemical XAS

AUTHOR(S):

ORIKASA, Yuki; INA, Toshiaki; YAMAMOTO, Kentaro; NAKAO, Takayuki; MINESHIGE, Atsushi; AMEZAWA, Koji; KAWADA, Tatsuya; TANIDA, Hajime; URUGA, Tomoya; UCHIMOTO, Yoshiharu

---

CITATION:

ORIKASA, Yuki ...[et al]. Direct Observation of Rate Determining Step for Nd<sub>2</sub>NiO<sub>4+δ</sub> SOFC Cathode Reaction by operando Electrochemical XAS. *Electrochemistry* 2014, 82(10): 897-900

ISSUE DATE:

2014-10

URL:

<http://hdl.handle.net/2433/191120>

RIGHT:

© 2014 The Electrochemical Society of Japan; This is not the published version. Please cite only the published version.; この論文は出版社版でありません。引用の際には出版社版をご確認ご利用ください。

# Direct Observation of Rate Determining Step for $\text{Nd}_2\text{NiO}_{4+\delta}$ SOFC Cathode

## Reaction by *operando* Electrochemical XAS

Yuki ORIKASA<sup>a, \*</sup>, Toshiaki INA<sup>a</sup>, Kentaro YAMAMOTO<sup>a</sup>, Takayuki NAKAO<sup>a</sup>,

Atsushi MINESHIGE<sup>b</sup>, Koji AMEZAWA<sup>c</sup>, Tatsuya KAWADA<sup>d</sup>, Hajime TANIDA<sup>e</sup>,

Tomoya URUGA<sup>e</sup>, Yoshiharu UCHIMOTO<sup>a</sup>

<sup>a</sup> Graduate School of Human and Environmental Studies, Kyoto University, Yoshida-nihonmatsu-cho, Sakyo-ku, Kyoto 606-8501 Japan

<sup>b</sup> Graduate School of Engineering, University of Hyogo, 2167 Shosha, Himeji 671-2280, Japan

<sup>c</sup> Institute of Multidisciplinary Research for Advanced Materials, Tohoku University, 2-1-1 Katahira, Aoba-ku, Sendai, Miyagi 980-8577, Japan

<sup>d</sup> Graduate School of Environmental Studies, Tohoku University, 6-6-04 Aramaki Aza Aoba, Aoba-ku, Sendai, Miyagi 980-8579, Japan

<sup>e</sup> Japan Synchrotron Radiation Research Institute (JASRI), 1-1-1, Kouto, Sayo-cho, Sayo-gun, Hyogo 679-5198, Japan

*\*Corresponding author; orikasa.yuuki.2a@kyoto-u.ac.jp*

## Abstract

The oxygen chemical potential of dense  $\text{Nd}_2\text{NiO}_{4+\delta}$  thin films on  $\text{Zr}_{0.92}\text{Y}_{0.08}\text{O}_{1.96}$  electrolyte was investigated by *operando* X-ray absorption spectroscopy (XAS) measurements. *Operando* XAS at the Ni *K*-edge was measured under an applied voltage and various oxygen partial pressures at high temperature to simulate the operating conditions of solid oxide fuel cells (SOFCs). The absorption edge energy under various polarizations is similar to those measured under equivalent oxygen partial pressures under open circuit condition. Thus, the oxygen chemical potential changes drastically at the electrode/gas interface and the rate-determining step of this model system is the surface reaction. This study provides direct evidence for the rate-determining step of the SOFC cathode reaction.

**Keywords:** Solid oxide fuel cells, Cathode,  $\text{Nd}_2\text{NiO}_4$ , *Operando* XAS

## 1. Introduction

High-temperature solid-state ionic devices such as solid-state oxide fuel cells (SOFCs), oxygen-permeable membranes, and gas sensors have attracted considerable attention as energy efficient systems.<sup>1-4</sup> To improve their performance, it is important to understand the electrochemical reaction mechanisms, including the rate-determining step (e.g., oxide ion diffusion and electron redox) during device operation. The reaction around electrodes is believed to consist of various elementary steps. For example, the electrode reactions of SOFC cathodes consist of gas diffusion in the gas phase, surface reactions at the gas/electrode interface, bulk diffusion inside the electrode, and ion transfer at the electrode/electrolyte interface.<sup>5</sup> Although it is important to identify the rate-determining step amongst these reactions, many details are still poorly understood.

To understand the electrode reaction mechanism of high-temperature electrochemical devices, AC impedance and DC polarization measurements are typically used.<sup>5, 6</sup> In these methods, the mechanism is determined from the relationship between the energy measured as the electrochemical potential and the reaction rate measured as the current density. It is essential to understand the physical/chemical

states of the electrode and electrolyte under operating conditions, as this should provide detailed information about the reaction mechanism, especially for the rate-determining step. However, chemical state measurements during the operation of high-temperature electrochemical devices are extremely difficult to obtain, because these devices operate under extreme conditions.

In general, an overpotential is applied to the rate-determining step, which changes the oxygen chemical potential of the SOFC cathode reactions. For most cathode materials in SOFCs, the introduction of oxygen vacancy is compensated for by the valence change of a 3d transition metal. This means the valence change corresponds directly to the change of oxygen chemical potential.<sup>7</sup> This study utilizes X-ray absorption spectroscopy (XAS) to investigate the valence change of 3d transition metals. XAS can be a potent and versatile technique for *operando* measurements under operating conditions such as applied polarization, high temperatures, and various gas atmospheres.

This study aims to identify the rate-determining step of the cathode reaction of SOFCs. We chose the neodymium nickel oxide ( $\text{Nd}_2\text{NiO}_{4+\delta}$ )/yttrium-doped zirconia

(YSZ) system as a model system for SOFC cathodes. This is because  $\text{Nd}_2\text{NiO}_{4+\delta}$  is a promising cathode material owing to its high mixed ionic-electronic conductivity and moderate thermal expansion coefficient.<sup>8, 9</sup> Dense  $\text{Nd}_2\text{NiO}_{4+\delta}$  thin films were prepared by pulsed laser deposition. *Operando* XAS at the Ni *K*-edge was measured under an applied voltage and various oxygen partial pressures at high temperatures. The oxygen chemical potential change of  $\text{Nd}_2\text{NiO}_{4+\delta}$  and the rate-determining step of the cathode reaction are discussed.

## 2. Experimental

$\text{Nd}_2\text{NiO}_{4+\delta}$  powders were prepared by the Pechini method.<sup>7, 10, 11</sup> The powders were pressed into pellets and sintered at 1573 K for 10 h in air. The pellets were annealed at 1073 K for 4 h under the desired oxygen partial pressures ( $p(\text{O}_2)$ ). Oxygen partial pressures during annealing were maintained at  $10^5$ ,  $10^4$ ,  $10^3$ ,  $10^2$ , or 10 Pa by purging high-purity  $\text{O}_2$  or  $\text{Ar}/\text{O}_2$  gas mixtures. The oxygen content of the samples was determined by iodometric titration. Details of the iodometric titration of the samples are described elsewhere.<sup>12</sup>

$\text{Nd}_2\text{NiO}_{4+\delta}$  thin films were prepared by the pulsed laser deposition (PLD) method using a YAG laser ( $\lambda = 256$  nm, pulse energy = 0.15 W). YSZ ( $\text{Zr}_{0.92}\text{Y}_{0.08}\text{O}_{1.96}$ ) powders (TZ-8Y, Toso Co.,Ltd., Japan) were cold-isostatically pressed at 200 MPa and sintered at 1773 K for 24 h. The pellets were mirror-polished with a diamond paste and used as the substrate. The base pressure in the chamber was maintained below  $10^{-3}$  Pa. Deposition at a frequency of 10 Hz was performed for 3 h at a substrate temperature of 1073 K. Films were deposited under pure oxygen at a pressure of 1 Pa. X-ray diffraction patterns were obtained using Cu-K $\alpha$  radiation (Rigaku, RINT-2200). A transmission electron microscope (TEM) (HF-2000 HITACHI) was used to determine the surface morphology of the  $\text{Nd}_2\text{NiO}_{4+\delta}$  thin films.

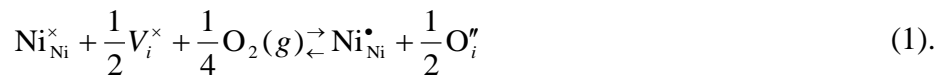
XAS measurements at the Ni *K*-edge were performed at beamline BL01B1 of SPring-8 at the Japan Synchrotron Radiation Research Institute (JASRI) in Sayo, Japan. Schematic view of cell configuration for *operando* electrochemical XAS measurements is shown in Fig. 1. A three electrode cell approximately 5 mm in diameter was prepared.  $\text{Nd}_2\text{NiO}_{4+\delta}$  thin films were used as the working electrode while porous platinum was used in both the counter and reference electrodes. To estimate the IR drop due to

electrolyte resistance, impedance measurements were performed over the frequency range 10 kHz–0.1 Hz using a potentiostat (Princeton VersaSTAT3). The electrode overpotential was calculated by subtracting the IR drop from the applied voltage. Ni *K*-edge X-ray absorption near edge structure (XANES) spectra were measured in the fluorescence mode. Incident X-ray enters the thin films from the top side. The penetration length of X-ray at Ni *K*-edge is much more than 1  $\mu\text{m}$  which is much longer than film thickness. The self-absorption effect is negligible because of using the thin film samples. Measurements under the open circuit condition were performed at 973 K under various oxygen partial pressures [ $p(\text{O}_2) = 10, 10^2, 10^3, 10^4$ , and  $10^5$  Pa]. Measurements under constant polarizations of -0.21, -0.115, 0, 0.075, or 0.155 V were also performed at 973 K under an oxygen partial pressure of  $10^3$  Pa. In this study, the absorption edge energy is defined as the energy at half the maximum intensity of the absorption edge.

### 3. Results and Discussion



The effectiveness of XAS analysis for the estimation of oxygen chemical potential in  $\text{Nd}_2\text{NiO}_{4+\delta}$  was examined. Figure 2 shows the Ni *K*-edge XANES spectra of  $\text{Nd}_2\text{NiO}_{4+\delta}$  annealed under various oxygen partial pressures. The absorption edge shifted toward lower energy with decreasing oxygen partial pressures. Shifts in the absorption edge energy are related to electronic structural changes, mainly caused by a change in the valence state of the absorbing atoms.<sup>13, 14</sup>  $\text{Nd}_2\text{NiO}_{4+\delta}$  exhibits nonstoichiometry depending on the oxygen partial pressure.<sup>15-17</sup> A decrease in the oxygen content of  $\text{Nd}_2\text{NiO}_{4+\delta}$  leads to a concomitant decrease in the mean Ni valence, due to charge compensation. The shift toward lower energy in the Ni *K*-edge XANES measurements corresponded to a decrease in the formal valence of Ni. Our XANES measurements indicate that the defect chemistry of  $\text{Nd}_2\text{NiO}_{4+\delta}$  can be described by the following Kröger-Vink notation:



Since the oxygen chemical potential correlates directly with the oxygen content, the oxygen chemical potential can be evaluated by XANES analysis of the  $\text{Nd}_2\text{NiO}_{4+\delta}$  system.

Figure 3 shows the XRD pattern and TEM micrograph cross-section of a  $\text{Nd}_2\text{NiO}_{4+\delta}$  thin film on the YSZ substrate. For the XRD pattern, only diffraction peaks from the orthorhombic  $\text{Nd}_2\text{NiO}_{4+\delta}$  phase and the cubic YSZ phase were observed. The film thickness was approximately 100 nm and the dense thin film deposition was confirmed. The electrode reaction of mixed ionic conductors consists of various elementary reactions. If dense thin films are used as electrodes, we do not have to consider the effect of surface diffusion. This is because the reaction path is limited to oxide ion transport through the electrode film. The prepared system is an appropriate model to analyze the rate-determining step of cathode reactions.

Ni *K*-edge XANES spectra were measured at various oxygen partial pressures under the open circuit condition, as well as with various DC biases under  $p(\text{O}_2) = 10^3$  Pa at 973 K (Fig. 4). The absorption edge shifted toward lower energy with decreasing oxygen partial pressures (Fig. 4(a)), consistent with the XANES results of bulk  $\text{Nd}_2\text{NiO}_{4+\delta}$  annealed under various oxygen partial pressures. Figure 4 (b) shows the *operando* XANES spectra at the Ni *K*-edge measured with various electrode

polarizations at 973 K under an oxygen partial pressure of  $10^3$  Pa. The electrode polarization voltage,  $\eta$ , was estimated using the equation below:

$$\eta = V_{\text{apply}} - R_{\text{bulk}} I \quad (2)$$

where  $V_{\text{apply}}$  is the potential between the working and the reference electrodes,  $R_{\text{bulk}}$  is the ohmic resistance between the working and the reference electrodes which can be from impedance spectroscopy measurements, and  $I$  is the current. The absorption edge peak of the Ni  $K$ -edge shifted toward lower energy with cathodic polarization (Fig. 4(b)). The edge peak shifted toward higher energy with anodic polarization. The shift corresponds to a concomitant decrease or increase in the formal valence of Ni due to the increment or decrement of interstitial oxygen (Equation (1)). Therefore, the oxygen chemical potential of the electrode changed with electrode polarization. Figure 5 shows the absorption energies measured under polarization in the oxygen partial pressure of  $10^3$  Pa and under the open circuit condition as a function of the effective oxygen partial pressure at the electrode/electrolyte interface,  $p(\text{O}_2)_{\text{int}}$ . The overpotential  $\eta$  can be regarded as a deviation of the oxygen chemical potential at the electrode/electrolyte

interface,  $\mu_{O,int}$ , from the oxygen potential in the gas phase,  $\mu_{O,gas}$  when assuming the

local equilibrium in the electrode and the electrolyte:<sup>18</sup>

$$2F\eta = \mu_{O,int} - \mu_{O,gas} \quad (3),$$

where  $F$  is the Faraday constant. By using the equation (3),  $p(O_2)_{int}$  is expressed as

follows:

$$p(O_2)_{int} = \exp\left(\frac{2\mu_{O,int}}{RT}\right) = p(O_2)\exp\left(\frac{4F\eta}{RT}\right) \quad (4),$$

where  $R$  and  $T$  are the gas constant and absolute temperature. The shift of absorption

energy under the open circuit condition is similar to the shift observed under the

polarization with an equivalent effective oxygen partial pressure. The penetration

length of the incident and fluorescence X-ray at Ni  $K$ -edge is much longer than 1  $\mu m$ .

Therefore, the results in Fig. 5 shows the effective oxygen chemical potential under the

polarization,  $\mu_{O,eff}$  is constant all through the electrode and equivalent to the oxygen

chemical potential at the electrode/electrolyte interface,  $\mu_{O,int}$ .

Next, we discuss the oxygen chemical potential around the electrode for SOFC

operation. Under the open circuit condition, the oxygen chemical potential in the

electrode is constant. If the partial pressure of oxygen changes, the oxygen chemical

potential at the electrode/electrolyte interface,  $\mu_{O,int}$ , depends only on the oxygen potential in the gas phase,  $\mu_{O,gas}$ . When polarizations are applied to the electrodes,  $\mu_{O,int}$  can be defined as the equation (3).<sup>18</sup> The oxygen chemical potential in the gas phase and at the electrode/electrolyte interface can be estimated after defining these parameters. However, the oxygen chemical potential inside the electrode ( $\mu_{O,eff}$ ) remains unclear. As shown in Fig. 6 (a), the cathode reaction of dense electrodes involves (i) gas diffusion in the gas phase, (ii) surface reaction at gas/electrode interface, (iii) bulk diffusion inside the electrode, and (iv) ion transfer at the electrode/electrolyte interface. The  $\mu_{O,eff}$  profile depends on which process is the rate-determining step, as shown in Fig. 6 (b). If the surface reactions are the rate-determining step, the oxygen potential should then drop at the electrode surface, as shown in (ii). In contrast, when the electrode reaction is governed by bulk diffusion or ion transfer at the electrode/electrolyte interface, the oxygen potential profile should be as shown in (iii) or (iv), respectively (Fig. 6 (b)). Thus, if the surface reactions are the rate-determining step [Fig. 6 (b) (ii)], the oxygen chemical potential equivalently changes with the oxygen partial pressure under the open circuit condition. If, on the other hand, the ion

transfer at the electrode/electrolyte interface is the rate-determining step [Fig. 6 (b) (iv)], the oxygen chemical potential does not change with the effective oxygen partial pressure. Finally, if bulk diffusion is the rate-determining step [Fig. 6 (b) (iii)], the change of oxygen potential should be less than the value under the open circuit condition. Given that the oxygen chemical potential inside the electrode,  $\mu_{O,eff}$  is equal to the oxygen chemical potential at the electrode/electrolyte interface,  $\mu_{O,int}$  under the polarization, we can determine that the oxygen chemical potential under various polarizations and oxygen partial pressures changes significantly at the gas/electrode interface. Such findings lead us to conclude that surface reactions such as oxygen adsorption or ionization are the rate-determining step of the  $Nd_2NiO_{4+\delta}$ /YSZ model electrode. The impedance analysis of the epitaxial  $Nd_2NiO_{4+\delta}$  thin film reported the charge transfer at gas/electrode interface is rate-determining step.<sup>19</sup> Previously, the impedance measurement and the isotopic exchange depth profile coupled with secondary ion mass spectroscopy measurement implied the rate-determining step is surface reaction for (La, Sr)CoO<sub>3</sub> system.<sup>18, 20</sup> The experimental results in this study are in good agreement with the previous studies and provide direct evidence for the rate-

determining step of surface reactions in SOFC cathode reaction. Enhancing surface reactions is the most important strategy for further improvement of cathode materials.

#### 4. Conclusion

Dense  $\text{Nd}_2\text{NiO}_{4+\delta}$  thin film/YSZ model electrodes prepared by PLD were investigated using *operando* electrochemical XAS measurements. We successfully observed changes in the valence states of  $\text{Nd}_2\text{NiO}_{4+\delta}$  under SOFC operating conditions. The absorption edge shift of Ni *K*-edge XANES under various polarizations is commensurate to that under equivalent partial pressures of oxygen. The results reveal that the oxygen chemical potential changes under polarization at the electrode/gas interface. We clearly show that the surface reaction is the rate-determining step of the  $\text{Nd}_2\text{NiO}_{4+\delta}$ /YSZ model electrode.

## REFERENCES

1. A. Atkinson, S. Barnett, R.J. Gorte, J.T.S. Irvine, A.J. McEvoy, M. Mogensen, S.C. Singhal, J. Vohs, *Nat. Mater.*, **3**, 17 (2004).
2. H.J.M. Bouwmeester, *Catal. Today*, **82**, 141 (2003).
3. P.V. Hendriksen, P.H. Larsen, M. Mogensen, F.W. Poulsen, K. Wiik, *Catal. Today*, **56**, 283 (2000).
4. B.C.H. Steele, A. Heinzl, *Nature*, **414**, 345 (2001).
5. S.B. Adler, *Chem. Rev.*, **104**, 4791 (2004).
6. F.S. Baumann, J. Fleig, G. Cristiani, B. Stuhlhofer, H.U. Habermeier, J. Maier, *J. Electrochem. Soc.*, **154**, B931 (2007).
7. Y. Orikasa, T. Ina, T. Nakao, A. Mineshige, K. Amezawa, M. Oishi, H. Arai, Z. Ogumi, Y. Uchimoto, *J. Phys. Chem. C*, **115**, 16433 (2011).
8. T. Nakamura, K. Yashiro, K. Sato, J. Mizusaki, *Solid State Ionics*, **181**, 402 (2010).
9. A. Egger, E. Bucher, W. Sitte, *J. Electrochem. Soc.*, **158**, B573 (2011).
10. Y. Orikasa, T. Ina, T. Nakao, A. Mineshige, K. Amezawa, M. Oishi, H. Arai, Z. Ogumi, Y. Uchimoto, *Phys. Chem. Chem. Phys.*, **13**, 16637 (2011).



11. Y. Oriksa, T. Nakao, M. Oishi, T. Ina, A. Mineshige, K. Amezawa, H. Arai, Z. Ogumi, Y. Uchimoto, *J. Mater. Chem.*, **21**, 14013 (2011).
12. J.W. Murray, L.S. Balistrieri, B. Paul, *Geochim. Cosmochim. Acta*, **48**, 1237 (1984).
13. J. Blasco, B. Aznar, J. Garcia, G. Subias, J. Herrero-Martin, J. Stankiewicz, *Phys. Rev. B*, **77**, 054107 (2008).
14. M.C. Sanchez, J. Garcia, J. Blasco, G. Subias, J. Perez-Cacho, *Phys. Rev. B*, **65**, 144409 (2002).
15. T. Nakamura, K. Yashiro, K. Sato, J. Mizusaki, *Solid State Ionics*, **180**, 1406 (2009).
16. T. Nakamura, K. Yashiro, K. Sato, J. Mizusaki, *J. Solid State Chem.*, **182**, 1533 (2009).
17. Y. Toyosumi, H. Ishikawa, K. Ishikawa, *J. Alloy. Comp.*, **408-412**, 1200 (2006).
18. T. Kawada, J. Suzuki, M. Sase, A. Kaimai, K. Yashiro, Y. Nigara, J. Mizusaki, K. Kawamura, H. Yugami, *J. Electrochem. Soc.*, **149**, E252 (2002).
19. A. Yamada, Y. Suzuki, K. Saka, M. Uehara, D. Mori, R. Kanno, T. Kiguchi, F. Mauvy, J.-C. Grenier, *Adv. Mater.*, **20**, 4124 (2008).

20. R.E. van Doorn, I.C. Fullarton, R.A. de Souza, J.A. Kilner, H.J.M. Bouwmeester,  
A.J. Burggraaf, *Solid State Ionics*, **96**, 1 (1997).

## FIGURE CAPTIONS.

**Figure 1.** Schematic illustration of the electrode geometry for *operand* electrochemical XAS measurements. The  $\text{Nd}_2\text{NiO}_{4+\delta}$  thin film was used as a working electrode. Circular Pt wire was contacted to the  $\text{Nd}_2\text{NiO}_{4+\delta}$  thin film by Pt paste as a current collector. The counter electrode was porous Pt. Pt wire was adhered using Pt paste as the reference electrode on the side of the YSZ. The diameter of the  $\text{Nd}_2\text{NiO}_{4+\delta}$  electrode was  $\sim 5$  mm. An R-type thermocouple was located near the sample.

**Figure 2.** Ni *K*-edge XANES spectra of  $\text{Nd}_2\text{NiO}_{4+\delta}$  annealed under various oxygen partial pressures at 1073 K.

**Figure 3.** X-ray diffraction patterns of the  $\text{Nd}_2\text{NiO}_{4+\delta}$  thin film on YSZ substrate. TEM micrographs showing the cross-section of the  $\text{Nd}_2\text{NiO}_{4+\delta}$  thin film on the YSZ substrate.

NNO:  $\text{Nd}_2\text{NiO}_{4+\delta}$

**Figure 4.** (a) XANES spectra at the Ni *K*-edge of the  $\text{Nd}_2\text{NiO}_{4+\delta}/\text{YSZ}$  model electrode measured under various oxygen partial pressures under the open circuit condition at 973 K. (b) Ni *K*-edge XANES spectra of the  $\text{Nd}_2\text{NiO}_{4+\delta}/\text{YSZ}$  model electrode measured under applying various biases at an oxygen partial pressure of  $10^3$  Pa at 973 K.

**Figure 5.** Absorption edge shift at the Ni *K*-edge of the  $\text{Nd}_2\text{NiO}_{4+\delta}/\text{YSZ}$  model electrode as a function of the effective oxygen pressure. Open squares show the shift measured under various oxygen partial pressures ( $p(\text{O}_2)$ ) values under the open circuit condition. Cross symbols show the shift measured with various DC biases at  $p(\text{O}_2) = 10^3$  Pa.

**Figure 6.** (a) Schematic illustration of elementary electrode reactions at the dense electrode/electrolyte interface for SOFC cathode reactions; (i), (ii), (iii), and (iv) represent the gas diffusion, surface reactions, bulk diffusion, and boundary transfer, respectively. (b) Schematic illustration of oxygen chemical potential profiles around dense electrodes. When voltage is applied to the electrodes, the oxygen chemical

potential at the electrode/electrolyte interface shifts; (ii), (iii), and (iv) correspond to the oxygen potential changes when the rate-determining step is the surface reaction, bulk diffusion, and boundary transfer, respectively.

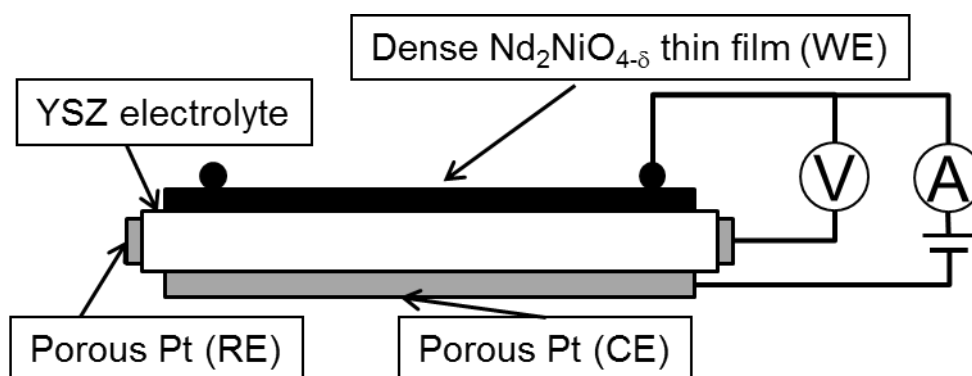


Fig. 1 Orikasa et al.

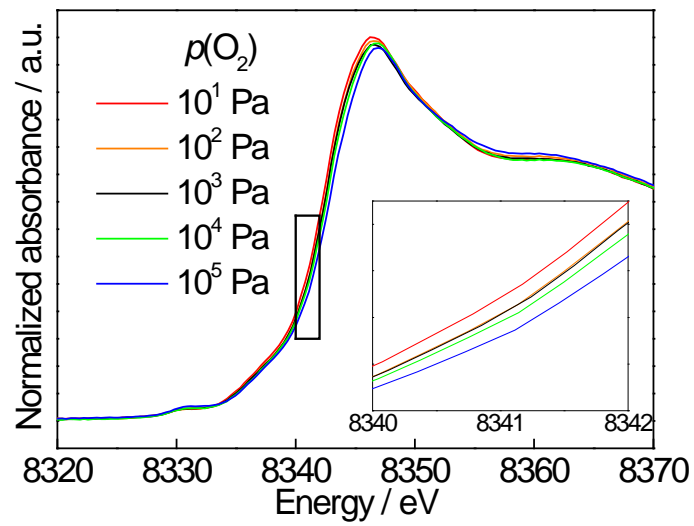


Fig. 2 Orikasa et al.

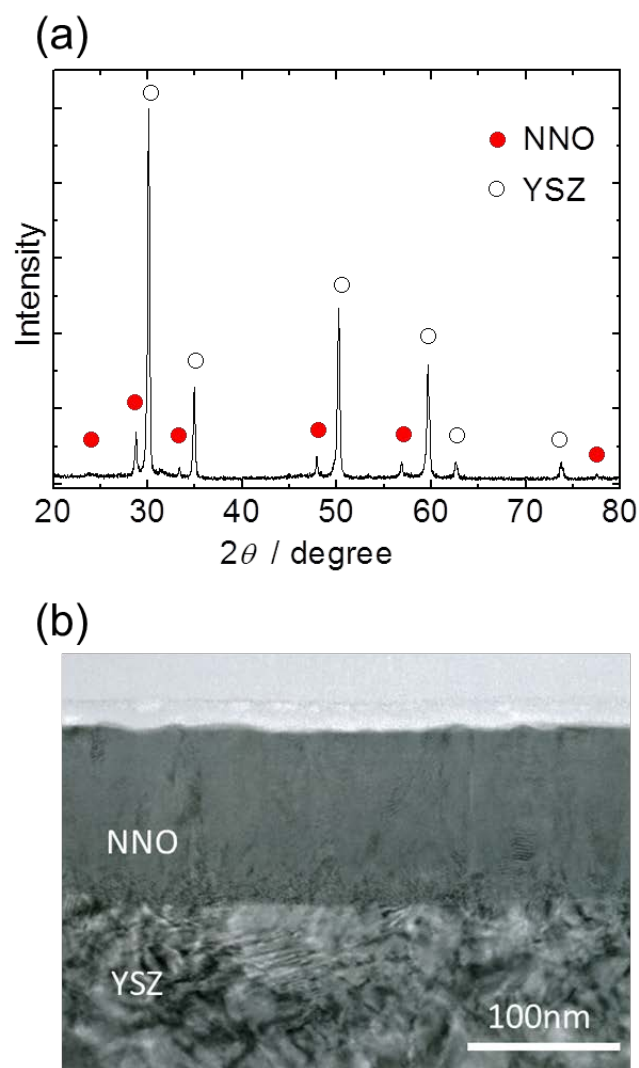


Fig. 3 Orikasa et al.



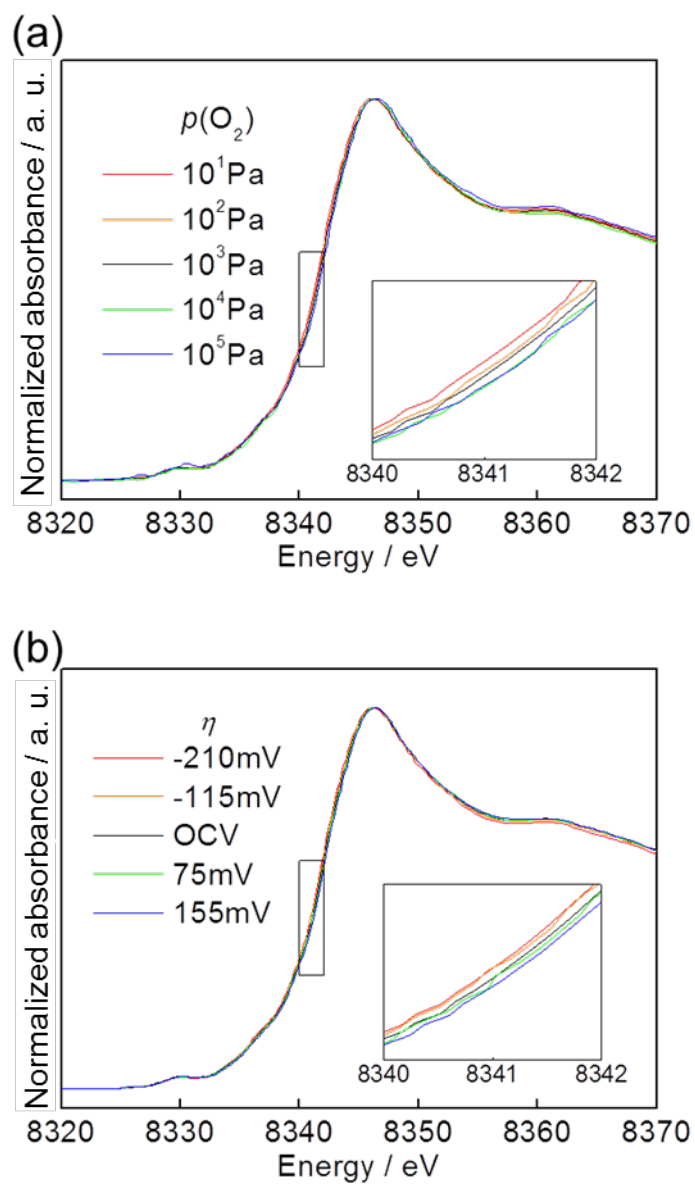


Fig. 4 Orikasa et al.

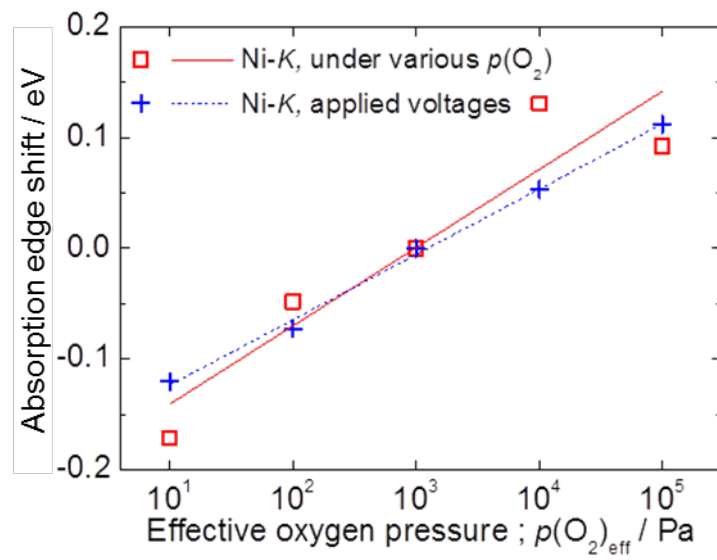


Fig. 5 Orikasa et al.

